Enhanced permeation by amphiphilic surfactant is spatially heterogenous at membrane and cell level

Robert Cavanagh[a^], Saif Shubber[a^], Driton Vllasaliu[b], Snjezana Stolnik[a*]

[a] School of Pharmacy, University of Nottingham, University Park, Nottingham NG7 2RD, UK

[b] School of Cancer & Pharmaceutical Sciences, Faculty of Life Sciences & Medicine, King's College London, Franklin-Wilkins Building, 150 Stamford Street, London SE1 9NH, UK

^ authors equally contributed

* corresponding author: snjezana.stolnik@nottinghma.ac.uk

Abstract

In the context of increased interest in permeability enhancement technologies to achieve mucosal delivery of drugs and biologics, we report our study on effects of the amphiphilic surfactant at cell membrane and cell population levels. Our results show that modulation in membrane order and fluidity initially occurs on insertion of individual surfactant molecules into the outer leaflet of membrane lipid bilayer; a process occurring at concentrations below surfactant's critical micellar concentration. The surfactant insertion, and consequent increase in membrane fluidity, are observed to be spatially heterogenous, i.e. manifested as 'patches' of increased membrane fluidity. At the cell population level, spatially heterogeneous activity of surfactant is also manifested, with certain cells displaying high permeability amongst a 'background' population. We propose that this heterogeneity is further manifested in a broad profile of intracellular and nuclear exposure levels to a model drug (doxorubicin) observed in cell population. The study points to heterogeneous nature of surfactant effects at cell membrane and cells in population levels.

Key words: permeability enhancement, amphiphilic surfactant, non-ionic surfactant, liposomes.

1. Introduction

The mucosal drug administration, including oral, lung or nasal routes, is normally a preferred option to achieve systemic drug therapy. In addition, drug delivery to epithelial cells comprising mucosal surfaces is currently receiving increased attention in potential treatments

of pulmonary or diseases of intestinal tract. Efficient mucosal delivery is however challenging due to the highly effective barrier presented by mucosal tissues [1-3]. Different strategies have been investigated and employed in attempts to enhance drug delivery into, or transport across, particularly of biologics, cell at mucosal surfaces [4]. Amongst other approaches these include a variety of, so called, permeability enhancers [5, 6], technologies often based on surfactant-type amphiphilic molecules. It has been extensively reported that application of amphiphilic surfactants increase the permeability of epithelial cell layer barriers to different permeants (e.g. small drug molecules and biologics) [7, 8], including our previous work [9, 10], and this approach has been adopted in some recently approved pharmaceutical products [11].

It is generally accepted that the amphiphilic surfactant-based permeability enhancers exert their action on cellular membrane of mucosal epithelial cells. However, our mechanistic understanding of the process, which would decipher details of the mechanism(s) by which membrane permeability enhancement by an amphiphilic surfactant is achieved, is still deficient. A contributing factor to this is the fact that cell plasma membrane is a complex structure evolved to regulate entry and exit of material into and out of the cell [12]. The fluid mosaic model [13], developed to describe the complexity of the plasma membrane, assumes that proteins embedded within the phospholipid bilayer are free to laterally diffuse throughout the bilayer and that potential interactions existing between lipids and proteins are non-specific. Some recent works suggest that lipid-lipid, lipid-protein and protein-protein interactions regulate phase separation within the membrane [14-18]. They introduce a concept of a highly ordered membrane 'patches', termed lipid rafts, which are compositionally and physically distinct from the surrounding 'disordered' areas, in terms of lipid packing, viscosity and protein composition [16]. This phase separation within the cell membrane is believed to compartmentalise many cellular processes including membrane trafficking, cellular organisation, and signalling facilitated by membrane proteins [17].

Studies have demonstrated that when exogenously applied material, including amphiphilic surfactant, interacts with the cell membrane, the plasma membrane's distinctive structure can be altered, which in turn modulates its functioning [19-22]. Our mechanistic understanding of these processes arrives primarily from studies on interactions of amphiphilic surfactants with cell membrane models, which are typically planar or liposomal phospholipid bilayers [23-25 26 27-29]. However, the composition of these model bilayers often comprises (almost entirely) of phosphocholine-type lipids, and this does not represent the compositional complexity of cellular membrane lipid bilayer. On the other hand, studies conducted using *in vitro* cells cultures normally report on the events which are consequent to membrane induced change (e.g. effective permeability P_{eff}) and provide little mechanistic understanding.

Here we present our study conducted in parallel, as technically feasible, in airway epithelial cells and a model cell membrane – giant liposomes with a bilayer lipid composition modelling that of epithelial plasma membrane. The study focuses on observations of spatial effects that exposure to an amphiphilic surfactant has on a model, complex composition lipid bilayers, and at cell membrane and cells in population levels. The amphiphilic surfactant,

Kolliphor® HS15, utilised in this work belongs to the macrogol family of non-ionic surfactants used as solubilizing excipients in oral and injectable pharmaceutical formulations [30]. Previous studies demonstrated that Kolliphor® HS15 promotes permeability across epithelial layers [31], and indicate that this may be a consequence of its interactions with cell membrane and consequent effects on the cell [10].

2. Materials and methods

2.1 Materials and cell culture

Amphiphilic surfactant, Kolliphor® HS15, used in this work is a mixture of polyglycol mono- and di-esters of 12 hydroxystearic acid; it was supplied by BASF. 6-Dodecanoyl-N,N-dimethyl-2-naphthylamine (Laurdan), calcein (mixed isomers), Hoechst 33258, well as 4-(2-hydroxyethyl)-1-piperazineethanesulfonic acid (HEPES), L-α-phosphatidylcholine (egg yolk), phosphatidylethanolamine (bovine brain), phosphatidylserine (bovine brain), phosphatidylinositol sodium salt (soy bean), sphingomyelin (bovine brain) and cholesterol were all purchased from Sigma Aldrich (UK). Rhodamine labelled phosphatidylethanolamine (Rho-PE) was purchased from Avanti Polar lipids (USA). DiIC18 (3H-Indolium, 2-[3-(1,3-dihydro-3,3-dimethyl-1-octadecyl-2H-indol-2-ylidene)-1-propenyl]-3,3-dimethyl-1-octadecyl-, perchlorate) and Bodipy-PC were purchased from Invitrogen Life Sciences.

Calu-3 cells were obtained from the American Type Culture Collection (ATCC) and used at passages 21-41. Cells were routinely cultured using Eagle's Minimum Essential Medium (EMEM, LGC standards, UK) supplemented with penicillin (100 units/ml), streptomycin (0.1 mg/ml), amphotericin (0.25 µg/ml) and Foetal Bovine Serum (FBS, 10% v/v). For experiments on cells, unless otherwise stated, Calu-3 cells were from its culture seeded into a black 96 well plate (Nucleon) at a seeding density of 10,000 cells *per* well. The plate was placed in incubator at 37 °C and 5 % CO_2 and cells nourished with complete Eagles minimum essential media (EMEM) for a minimum of 24 hours prior to their use. Cells were then washed three times with PBS and 200 µL Kolliphor® HS15 solutions at concentrations ranging from 0.01 – 5.2 mM prepared in HBSS/HEPES (25.0 mM, pH 7.4) medium were applied for 180 minutes at 37 °C.

2.2 Effect on cell membrane lipid domains

For this experiment, following surfactant exposure cells were washed three times using PBS and incubated for 30 minutes at 37 °C with a cocktail of Hoechst 33342 (25 µg/mL), BODIPY PC (6.0 µM), and DiIC18 (6.0 µM) in HBSS/HEPES. Cells were washed extensively and imaged using an EVOS® FL colour imaging microscope at 20X magnification using the DAPI ($\lambda_{ex/em}$ 360/447 nm), GFP ($\lambda_{ex/em}$ 480/525 nm), RFP ($\lambda_{ex/em}$ 530/593 nm) channels. The negative control in this experiment was HBSS/HEPES (25.0 mM, pH 7.4) alone. The fluorescent probes applied partition in different lipid domains: Dil C18 (red) has been shown to partition preferentially with saturated, long tailed phospholipids and

thus labels Lo regions [32], while BODIPY-PC (green) partitioning into L_D regions due to its bulky moiety on the fatty acid acyl chain [33].

2.3 Effect on fluidity of cell membrane

Calu-3 cells seeded in wells, as described above, were incubated with solution of Laurdan probe (100 nM) in HBSS/HEPES medium (25 mM, pH 7.4 for 30 minutes. Cells were then washed with PBS and solutions of Kolliphor® HS15 in HBSS/HEPES (pH 7.4 25 mM) were applied at different concentrations for 3 hours while cells were incubated at 37 or 4 °C. HBSS/HEPES medium was used as a negative control. Cells were washed with PBS, incubated with HBSS/HEPES and fluorescence emission read at $\lambda_{ex/em}$ 360/440 and 490 nm using a Tecan infinite 200 PRO multimode plate reader. Results are presented as generalised polarisation (GP) and were calculated using the following equation.

$$Generalised\ polarisation\ (GP) = \frac{(I_{440} - I_{490})}{(I_{440} + I_{490})}$$

For GP imaging, cells were incubated at 37 °C with Kolliphor® HS15 solutions in HBSS/HEPES (25 mM, pH 7.4) medium at the final surfactant concentrations ranging from 0.01 to 5.20 mM. Images were taken using a DMIRE2 florescence time-lapse microscope at excitation at wavelength $\lambda_{ex/em}$ 359/461 and 488 nm. At least 15 images were captured at each wavelength per treatment sample and used to create GP images applying ImageJ 1.47. Images were created using a macro for processing two channel Laurdan into GP images provided by Owen *et al.* [34]. Representative images are shown from three independent repeats (N=3).

2.4 Effect on the morphology of lipid bilayer in giant liposomes and cells

Giant liposomes were formed according to the lipid film rehydration method [35]. Required lipids (Supplementary Information Table S1) and rhodamine-labelled PE (0.1 mol% total lipid) were initially dissolved in a chloroform/methanol (2:1 %v/v) mixture and mixed in round bottom flask to achieve a 1 mg/mL total lipid solution. The solvent was evaporated under a stream of nitrogen gas to form the lipid film. The round bottom flask was then left to dry for six hours to ensure residual solvent was removed. Once the lipidic film was formed, 1.0 ml of pre-warmed (45 ^{o}C) HBSS/HEPES medium was added and incubated for 10 minutes at 45 °C. Following this, 4 mL 0.4 M sucrose solution (in HBSS/HEPES) was added, the flask sealed with N_2 gas, and incubated at 45 °C for 24 hours. Formed giant liposomes were mixed with solutions of the surfactant at various concentrations and single liposomes were imaged using an EVOS® FL colour imaging fluorescent microscope with wavelength set to $\lambda_{ex/em}$ 530/593 nm (100 X magnification). The microscopy analysis was performed at room temperature.

Parallel experiment was conducted in erythrocytes (obtained from Phlebotomy Department at Nottingham University Hospitals Trust), and cells exposed to surfactant imaged using SEM (JOEL 6400).

2.5 Effect on cell membrane cholesterol levels

Calu-3 cells, seeded as described above, were incubated with solutions of Kolliphor® HS15 in HBSS/HEPES medium at different concentrations for 3 hours at 37 °C. HBSS/HEPES medium and 4 mM β-methyl cyclodextrin solution were used as negative and positive controls, respectively. Next cells were washed with PBS and fixed using 4 % w/v paraformaldehyde for 10 minutes at room temperature. Cells were rinsed again and incubated with filipin solution in HBSS/HEPES (50 µg/mL) for 90 minutes at room temperature. Following staining with filipin, cells were washed extensively using PBS and fluorescence emission read at $\lambda_{ex/em}$ 364/480 nm using a Tecan infinite 200 PRO multimode plate reader. Cholesterol reduction was calculated normalised to the controls by setting as 0% cholesterol reduction value for incubation with HBSS/HEPES medium, and as 100% value induced by treatment with 4 mM solution of β-methyl cyclodextrin. For fluorescent imaging, test samples were prepared as above, and imaged using an EVOS® FL colour imaging fluorescent microscope.

2.6 Effect on LDH release

Following cells incubation with surfactant, as described above, supernatant was removed and LDH activity in medium assessed using an LDH cytotoxicity kit (Sigma TOX7, UK). Absorbance was read at 492 nm and absorbance values related to the induced LDH release from medium alone (0%) and Triton X-100 (3.2 mM solution) (taken as 100%) exposures:

$$Relative\ LDH\ release\ (\%) = \left(\frac{(HBSS{:}HEPES\ \ absorption - Triton\ x100\ \ absorption)}{(Sample\ \ absorption - Triton\ x100\ \ absorption)}\right)\ x\ 100$$

2.7 Calcein membrane permeability

Calu-3 cell layers were grown on Transwell® permeable supports, at a seeding density of $1.25x10^5$ cells *per* insert. The cells were cultured in a liquid covered fashion. Layer integrity was measured and confirmed by transepithelial electrical resistance (TEER) measurements. Cells with TEER values exceeding 500 Ωcm^2 were used for further experiments.

The study was performed in HBSS/HEPES buffer (25.0 mM, pH 7.4) at 37 °C. The cells were incubated with 1.5 mL (basal) and 0.5 mL (apical) HBSS/HEPES for 1 hour prior to the experiment. The apical solution was then withdrawn and a 0.25 mL solution of calcein (200 µg/mL) in HBSS/HEPES added. To this, 0.25 mL of HBSS/HEPES buffer was added for the negative control sample, or the same volume of surfactant solutions to achieve final treatment concentrations of 5.0, 1.0 and 0.01 mM. Samples were incubated for three hours at 37 °C and cells then washed three times with PBS. Cells were then fixed using 4% paraformaldehyde at room temperature (22 ^oC) for approximately 10 minutes. Following this, a 25 µg/mL Hoechst 33342 in PBS solution was added to the cells for 10 minutes at room temperature. Each insert was then washed with PBS extensively. Finally the filter membrane excised from the insert and mounted (80 % glycerol) on glass slides for confocal imaging. Cells were imaged using a Leica TCS SP2 system mounted on a Leica DMIRE2 inverted microscope, DAPI channel 358/461 nm and FITC channel 494/518 nm.

2.8 CellTox® nuclear membrane permeability

Nuclear membrane permeability was assessed by the binding of the cell impermeable CellTox Green dye (Promega) to nuclear DNA. Calu-3 cells were seeded in black 96 well plates (Corning) at a density of $1x10^4$ cells *per* well and culture for 48 hours prior to assaying. Surfactant solutions (0.05-5.0 mM) were prepared in HBSS/HEPES (25 mM, pH 7.4). HBSS/HEPES buffer was used as the negative control and 0.2% Triton X-100 in HBSS/HEPES applied as positive control to induce total cellular permeabilisation. Treatments were applied with 1% CellTox green dye and exposed to cells for 4 hours. Fluorescence was then measured at $\lambda_{ex/em}$ 495/519 nm using a Tecan Spark 10M plate reader.

To visualise changes in nuclear permeability, CellTox green uptake was imaged using fluorescence microscopy. Calu-3 cells were seeded in 12 well plates (Corning) at a density of $1.2x10^5$ cells *per* well and cultured for 48 hours. Treatments were prepared with 1% CellTox Green dye as described above and applied to cells for 4 hours. Cells were then washed twice with PBS and fixed with 4% PFA for 10 minutes at room temperature. Cellular imaging was then performed on an EVOS® FL colour imaging microscope at 20X magnification using the GFP ($\lambda_{ex/em}$ 470/525 nm) and brightfield channels, and images merged using Image J (v1.52f).

2.9 Doxorubicin cell internalization and potency

Doxorubicin (doxorubicin hydrochloride) cellular internalization was assessed using fluorescence microscopy and subsequent image analysis. For this experiment Calu-3 cells were seeded in 12 well plates (Corning) at a density of 1.2 $x10^5$ cells *per* well and cultured for 24 hours. Solutions containing doxorubicin (10 µM) and Kolliphor HS15 (0.01, 0.05 or 0.1 mM) were prepared in 10 % v/v FBS/DMEM medium and applied to cells for 1, 2 or 4 hours. Doxorubicin solution in 10 % v/v in FBS/DMEM medium served as the drug alone control. Following exposure, treatment solutions were removed and cells washed three times with PBS. DAPI (1 µg/mL) (ThermoFisher) nuclear stain diluted in PBS was applied for 15 minutes at 37°C. Cells were washed with PBS and then fixed with 4 % PFA for 10 minutes at room temperature. Imaging was performed on an EVOS® FL microscope using DAPI ($\lambda_{ex/em}$ 360/447 nm) and RFP ($\lambda_{ex/em}$ 530/593 nm) channels, for DAPI and doxorubicin detection, respectively. Images were merged using Image J (v1.52f) software. DAPI and doxorubicin fluorescent signals were quantified using ImageJ and a fluorescence intensity ratio (RFP/DAPI) was calculated to enable an estimation of doxorubicin internalization by cells normalised to nuclear signal. At least 200 nuclei were measured *per* group from three images from independent experiments.

The potency of doxorubicin ($1x10^{-4}$ - $1x10^2$ µM) applied with, or without Kolliphor HS15 (0.01 - 0.1 mM) was studied using the PrestoBlue cell viability assay (ThermoFisher) to measure cellular metabolic activity. Calu-3 cells were seeded in black 96 well plates (Corning) at a density of 10,000 cells *per* well and cultured for 48 hours prior to assaying. Treatments were diluted in 10 % v/v FBS/DMEM medium and applied to Calu-3 cells for 24 hours. The negative control used was 10 % FBS/DMEM alone and the positive cell death control was 0.2 % Triton X-100 solution in 10 % FBS/DMEM. Following exposure,

treatment solutions were removed, cells washed with PBS, and 100 µL *per* well of 10 % PrestoBlue reagent diluted in DMEM (no phenol red) was applied to cells for 60 minutes. Solution fluorescence was then measured at 560/600 nm ($\lambda_{ex}/\lambda_{em}$), and relative metabolic activity calculated by setting the values of the negative control as 100% and the positive control (0.2% Triton X-100) as 0%.

2.10 Statistical analysis

Dose-response curve fitting was performed using non-linear regression analysis to enable IC_{50} determination (GraphPad prism, version 7.03). All data are presented as mean ± S.D from triplicates of three independent experiments, unless stated otherwise. Microscope images shown are representative of at least three independent experiments. Statistical analysis was performed by one-way ANOVA with Tukey's multiple comparison post hoc test using GraphPad Prism.

3. Results

3.1 Modulation of cell plasma membrane lipid domains

Initial observation on activity of the amphiphilic surfactant on epithelial Calu-3 cells is depicted in Figure 1. The images visualise the fluorescence of probes employed; these preferentially localize in liquid ordered (L_O) (Dil C18, red) or liquid disordered (L_D) (BODIPY-PC, green) domains of plasma membrane. The images depict a surfactant concentration-dependent modulation in the cell membrane lipid domains, with increased presence of liquid disordered (L_D) domains (green) as the surfactant concentration is increased. In control conditions (no surfactant treatment) both liquid disordered (green) and liquid ordered (red) regions are observed. This surfactant effect on plasma membrane lipid domains was also observed in human fibroblast 3T3 cells (Supporting Information Figure S2). Images in Figures 1 and S2 further reveal differences in intensity of red/green florescence between individual cells in the population, indicating cell-to-cell heterogenicity in liquid order/disorder domains of their plasma membrane, including on surfactant exposure.

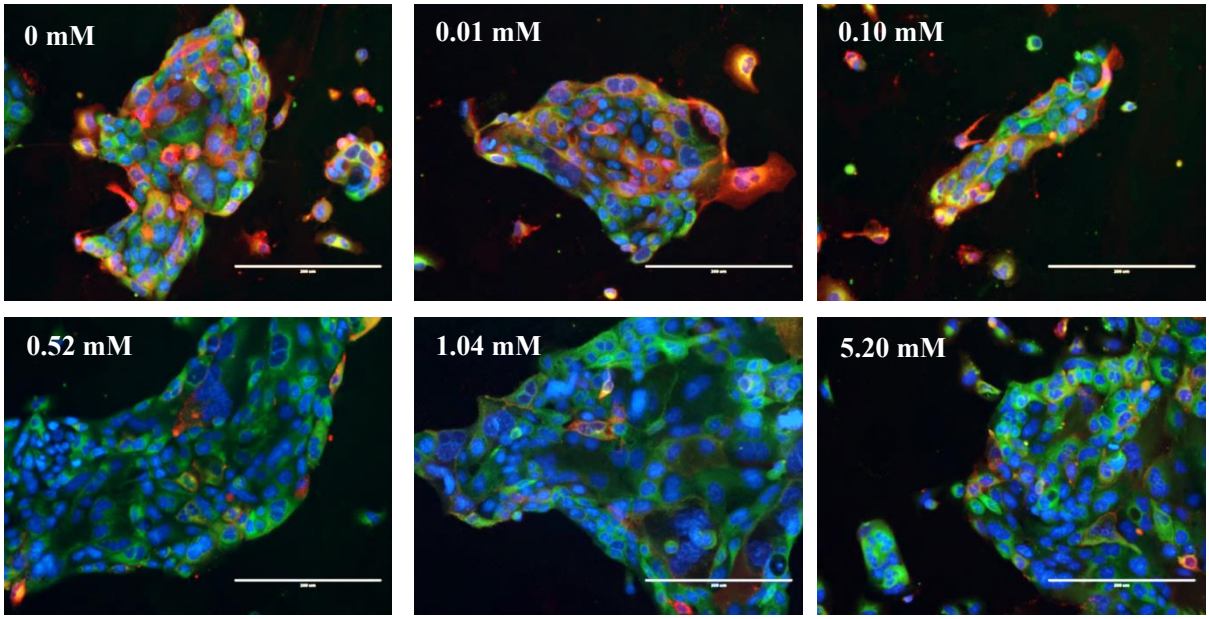

Figure 1. Fluorescent microscopy of Calu-3 cell plasma membrane lipid domains following exposure to amphiphilic surfactant. Calu-3 cells were incubated with different concentrations of amphiphilic surfactant, as indicated in individual images, for 180 minutes at 37 °C. Cells were stained with a cocktail of 25 µg/mL Hoechst 33342 (blue, nuclear stain), 6.0 µM BODIPY-PC (green) and 6.0 µM DiIC18 (red) and excitation/emission read using DAPI ($\lambda_{ex/em}$ 360/447 nm), GFP ($\lambda_{ex/em}$ 470/525 nm) and RFP ($\lambda_{ex/em}$ 530/593 nm) filters. Scale bar represents 200 µm.

3.2 Increased fluidity of cell plasma membrane

The membrane fluidity of Calu-3 cells exposed to surfactant was assessed by general polarization (GP) of Laurdan dye. Figure 2a depicts a statistically significant decrease in GP values in cell population, indicating a significant increase in plasma membrane fluidity, as the surfactant concentration in treatment solution increases. It should be noted that a statistically significant decrease in GP occurs at surfactant concentrations that are below the surfactant critical micellar concentration (CMC 0.05 – 0.1 mM). GP imaging of individual cells in Figure 2a visually illustrates that the observed increase in membrane fluidity upon surfactant exposure does not appear to be spatially homogeneously distributed; it is manifested preferentially at certain 'patches' at the plasma membrane. This was also observed in images of giant liposomes, where 'patches' of increased fluorescence (i.e. membrane fluidity) can be observed against the 'background' (Figure 2b). It should be noted that the lipid composition of the giant liposomes used in this study is modelled on that of epithelial cell membrane (Supporting Information Table S1), and that the surfactant concentrations tested are in the range relevant to Kolliphor HS15 concentrations achieved in human clinical trials [36]. Data at 180 minutes surfactant exposure are reported, as this exposure time resulted in measurable effects across the concentration range tested, i.e. below and above the surfactant CMC.

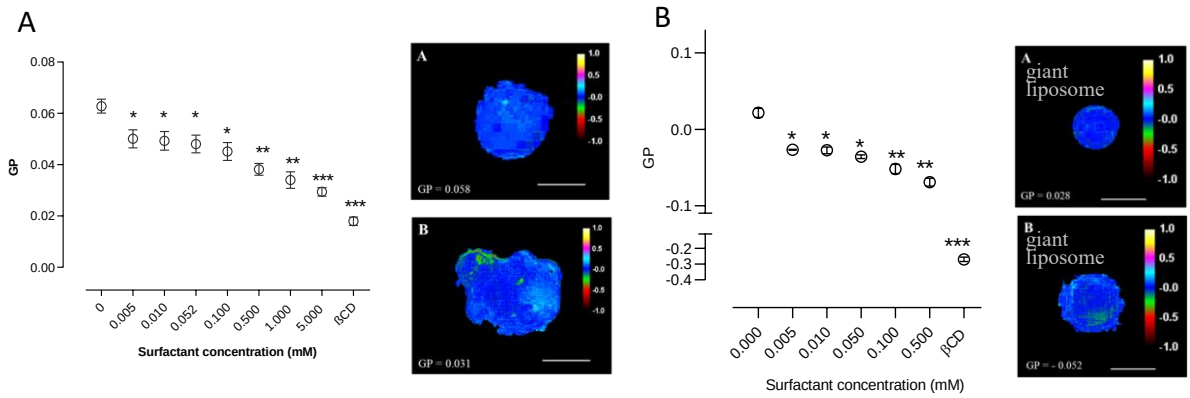

Figure 2. Membrane fluidity on exposure to surfactant solutions assessed by general polarisation (GP) of Laurdan dye. **a**) Effect of surfactant on Calu-3 plasma membrane Laurdan GP values. Surfactant solutions were applied for 3 hours at 37 °C; β-methyl cyclodextrin solution (4 mM) was used as a positive control. GP values calculated as described in experimental section. Right: Florescent imaging of untreated cells (image A) and cells treated with the 5.2 mM surfactant solution (image B). Scale bar represents 5 µm. **b**) GP values of giant liposomes exposed to increasing concentrations of the surfactant (as above). Right: Florescent imaging of untreated giant liposomes (image A) and treated with the 5.2 mM surfactant solution (image B). Scale bar represents 10 µm. Images taken at $\lambda_{ex/em}$ 359/461 and 488. GP images shown are representative from at least 15 images collected over three independent experiments and were created using image J 1.47 and a macro for processing two channel Laurdan into GP images was provided by Owen *et al.* [34]. Results displayed as mean GP value ± SD. N=3, n=3. * = P < 0.05, ** = P < 0.01 and *** = P < 0.001.

Data from a corresponding experiment conducted at 4°C (Supporting information, Figure S3) show that cells possess a higher GP value, indicating Laurdan probe localisation within an increased liquid ordered (L_O) phase, i.e. there is significantly reduced membrane fluidity relative to 37 °C conditions, which is in accordance with previous reports on temperature-dependence of membrane fluidity [37, 38]. It should be noted that at 4 °C the relative decreases in GP values upon surfactant exposure are less pronounced in comparison to those at 37 °C, indicating that the surfactant effect on membrane fluidity is a temperature-dependent process. It has been argued in previously reported studies that surfactants preferentially interact with membrane fluid phases,[39, 40] therefore an increase in liquid ordered phases at 4°C may consequently limits surfactant insertion and subsequent surfactant-mediated fluidisation observed in this experiment. In addition of temperature, it should be noticed that the surfactant effect on membrane fluidity is also time dependent (Supporting information, Figure S3).

3.3. Budding of lipid bilayer membrane

To assess if the observed increase in cell membrane fluidity can be, at least in part, credited to the insertion of surfactant molecules into the cell plasma membrane, we followed changes in membrane morphology of giant liposomes. As above, the lipid composition of the giant liposomes employed models that of epithelial cell membranes (Supporting information Table S1). Images in Figure 3 depict morphology of giant liposomes exposed to surfactant during 100 minutes of the experiment. The images reveal time-dependent changes, whereby it is important to notice that the first observable morphological change upon exposure to surfactant solution is budding of the liposomal membrane (membrane expanding outwards).

Budding on surfactant exposure was also observed in giant liposomes labelled with both Dil C18 and BODIPY-PC fluorescent probes (Supporting Information Figure S4). Eventually the extensive budding results in a gross restructuring of the membrane and formation of smaller, spherical 'vesicles'.

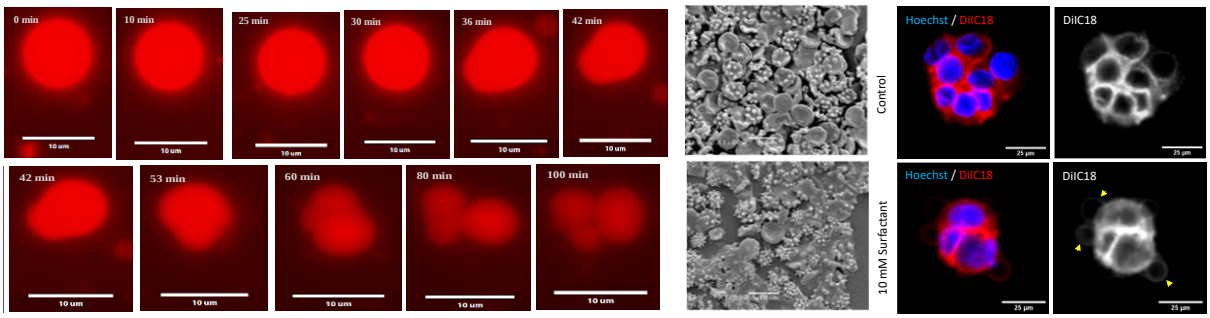

Figure 3: Membrane morphology in the presence of surfactant. Left: Representative time lapse images of a single liposome taken over 100 minutes at time points indicated in individual images. Liposomal lipid composition models membrane composition of epithelial cell plasma membrane (Supporting Information Table S1). Surfactant solution (5.0 mM) prepared in HBSS/HEPES buffer (pH 7.4, 25 mM). Scale bar 10 µm. Middle: Scanning electron microscopy images of erythrocytes exposed to surfactant. Cells were exposed to surfactant concentrations of 0.01(upper image) and 0.2 mM (lower image) for 2 hours at 37 ºC. A sub-populations of visibly 'affected' (echinocytic form) and not 'affected' (discocyte) erythrocytes are observed at lower concentration (upper image), whereby at the higher surfactant concentration (lower image) the 'spicules' are smaller and more numerous. Scale bar 10 µm. Control image of untreated cells in Supporting Information Figure S12. Right: Fluorescence microscopy of epithelial cells morphology in presence of surfactant. Representative images of cells treated with buffer (control) or 10 mM surfactant. Cells loaded with 10 µg/mL Hoechst 33342 and 6 µM DilC18 prior to treatment to stain nuclei (blue) and plasma membrane (red), respectively. Imaged using blue DAPI ($\lambda_{ex/em}$ 360/447 nm) and red RFP ($\lambda_{ex/em}$ 530/593 nm) filters. Arrows indicate membrane budding. Scale bar 25 µm.

In a further experiment (Figure 3), the cell membrane budding was observed in erythrocytes, with a sub-populations of affected (echinocytic form) and not affected (discocyte) erythrocytes present and, at higher surfactant concentration, 'spicules' which are smaller and more numerous. The literature proposes that echynocytic form is a consequence of amphiphilic compounds (eg. surfactants) incorporation at into outer leaflet of the membrane's lipid bilayer, producing a local area differences in the membrane bilayer which induce membrane 'budding' [41]. Membrane budding on exposure to surfactant was also observed in epithelial cells in culture, as indicated in fluorescence images in Figure 3.

3.4 Reduction in plasma membrane cholesterol level

To assess whether increases in cell membrane fluidity may also be arising from surfactant caused membrane depletion of cholesterol (a known regulator of membrane fluidity [41, 42]), cholesterol content of Calu-3 cell plasma membranes was determined *via* assessing intensity of filipin fluorescence [43]. Fluorescent imaging and spectrofluorescent measurements reveal

that surfactant exposure induces a reduction in plasma membrane cholesterol levels (Figure 4). This effect is statistically significant, relative to the buffer control, at surfactant concentrations > 0.10 mM, i.e. concentrations that lie above the surfactant CMC. As a positive comparison, β-methyl cyclodextrin (MβCD) was applied as a compound known to 'extract' cholesterol from the plasma membrane by forming soluble cholesterol inclusion complexes [31].

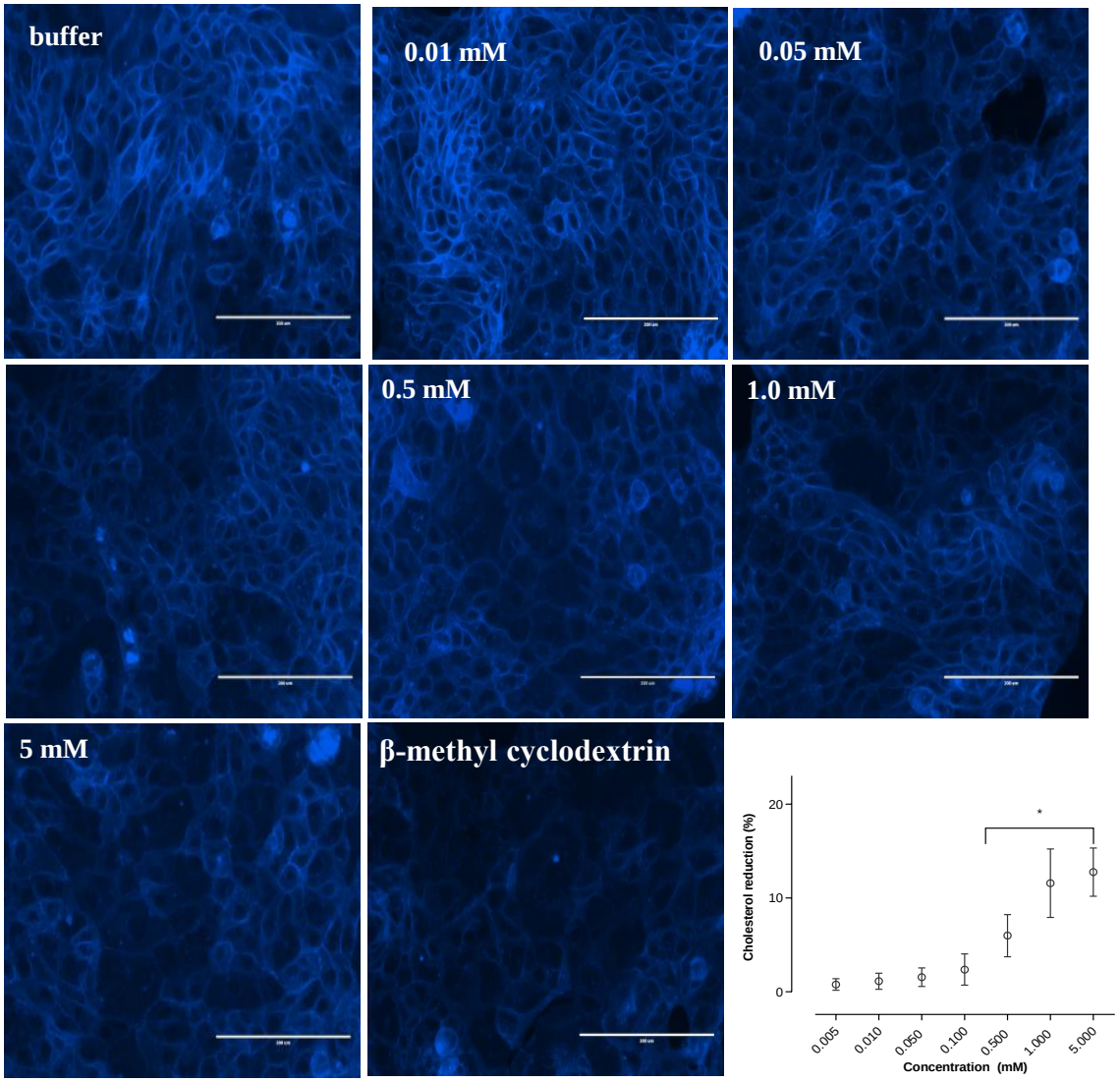

Figure 4. Fluorescence of filipin probe applied to assess cholesterol levels in Calu-3 cells following exposure to surfactant. a) Fluorescent microscopy images of filipin binding to Calu-3 plasma membrane cholesterol. Cells were exposed to the surfactant concentrations, as indicated in individual images, for 180 minutes at 37 °C. Untreated cells (buffer alone) and 4.0 mM β-methyl cyclodextrin were used as negative and positive controls, respectively. Following surfactant exposure, filipin was applied (76.4 µM for 90 minutes) and images taken using 20X magnification at $\lambda_{ex/em}$ 357/447 nm. Scale bar 200 µm. b) Quantitative assessment of Calu-3 cholesterol content following treatments (as above) *via* measurement of filipin fluorescence. Data

presented as mean ± S.D (N=3, n=3), and normalised to % cholesterol reduction as described in Materials and Methods section. *, $P < 0.05$.

3.5 Permeability across cell plasma and nuclear membranes

The effect of surfactant application on the integrity of cell plasma membrane was assessed by measuring extracellular release of lactose dehydrogenase enzyme (LDH) (Figure 5a). Results demonstrate concentration- and time-dependent release of LDH, indicating that a membrane perturbation induced by the surfactant is dependent on exposure conditions, in terms of both applied concentration and exposure time. Visualization of cell plasma membrane permeability in the Calu-3 cell population is shown in images in Figure 5b, as obtained using calcein (membrane-impermeable fluorescent probe) applied to differentiated cell layers. Untreated cell layer shows distribution of green calcein fluorescence mainly above and around the periphery of cells (depicted in Z-stacks), indicating its extracellular presence. At increased surfactant concentrations (1.0 and 5.0 mM) a spatially heterogeneous effect is observed in the cell population, where some cells display intense fluorescence, with confocal Z-stacks below the micrographs revealing intracellular presence of calcein (at level of cell nuclei). Considering surfactant effect on the nuclear membrane, data in Figure 5d illustrate increased nuclear membrane permeability to the CellTox fluorescent probe with an increase in surfactant concentration. In a similar manner to cell plasma membrane, images in Figure 5c show that this nuclear membrane permeability effect is heterogeneous in the cell population, whereby some cells display highly intense fluorescence.

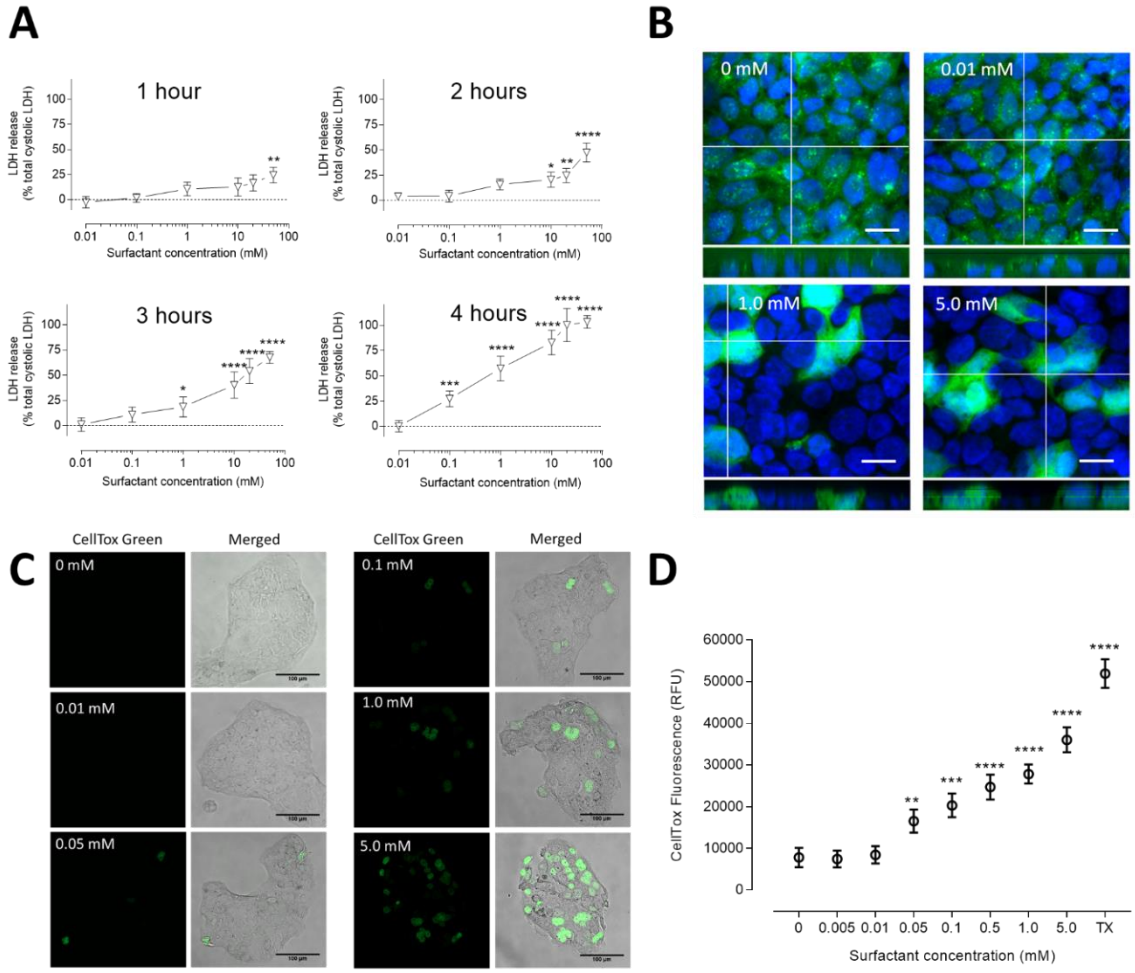

Figure 5. Effects of surfactant on Calu-3 cell plasma and nuclear membranes. A) Release of LDH for Calu-3 cells exposed to surfactant for 1, 2, 3 and 4 hours. Data are presented as relative values (%) following normalisation to buffer (0% LDH release) and 1% Triton X-100 (100% LDH release). Statistical significance determined via 2-way ANOVA and calculated against the vehicle control group. *p < 0.05, **p < 0.01, ***p < 0.001, ****p<0.0001. Data are presented as mean ± S.D. B) Visualisation of cell membrane permeability with cell membrane impermeable fluorescent probe calcein (0.32 mM). Calu-3 differentiated cell layers (Supporting Information, Figure S5A) were exposed to surfactant for 3 hours; cells imaged at $\lambda_{ex/em}$ 494/518 and $\lambda_{ex/em}$ 358/461 nm for calcein (green) and cell nuclei (blue DAPI). Scale bar represents 30 µm and cross hair represents region for Z stack analysis. C) Nuclear permeability in response to surfactant application. Fluorescent micrographs of the membrane impermeable DNA binding dye CellTox Green following 4 hours exposure to surfactant. Scale bars, 100 µm. Images with increased brightness for differential threshold detection shown in Supporting Information Figure S5B. D) Fluorescence of CellTox green measured *via* spectrofluorimetry following exposure to surfactant for 4 hours; buffer as negative control (0 mM) and 0.2% v/v Triton X-100 (TX) as positive control. Data presented as mean ± S.D. Statistical significance between treatment groups and the negative control (0 mM) determined via ANOVA followed by Dunnett's post hoc test. **p < 0.01, ***p < 0.001, ****p < 0.0001.

3.6 Enhancement of doxorubicin intracellular exposure and potency

Further to observed modulation of membrane permeability (Figure 5), and given the potential of surfactants to inhibit P-gp transporters [30, 31], we assessed the effects of the tested surfactant on doxorubicin cellular level and potency (Figure 6) and report nuclear level of doxorubicin in individual cells in population.

Images in Figure 6a demonstrate that treatment of Calu-3 cells with doxorubicin leads to its accumulation in cells nuclei, as indicated by co-localisation with the DAPI nuclear stain. Co-administration with surfactant increases the nuclear levels of doxorubicin, relative to doxorubicin alone (Figure 6a and 6b). This enhancement correlates with the increase in surfactant concentration and exposure time (Figure 6b), but shows that at higher contractions (0.05 and 0.1 mM) and longer exposure, particularly at 4 hours, nuclear doxorubicin levels show statistically significant decreases. This appears to corroborate with observed plasma membrane damage (seen in Figure 5) that occurs under similar exposure conditions.

Plots in Figure 6c present distribution profiles of nuclear levels of doxorubicin for doxorubicin treated cells exposed to surfactant at different concentrations and exposure times. Data indicate a clear shift to right with concentration and duration of surfactant exposure. i.e. higher doxorubicin level *per* nucleus indicating increased nuclear translocation of the drug. However, this increase in nuclear doxorubicin level varies in the cell population; i.e. wide distribution profiles at 2 and 4 hours suggest non-homogeneous levels of drug *per* nucleus in cells; an effect occurring for doxorubicin alone as well as for surfactant and doxorubicin co-administration groups.

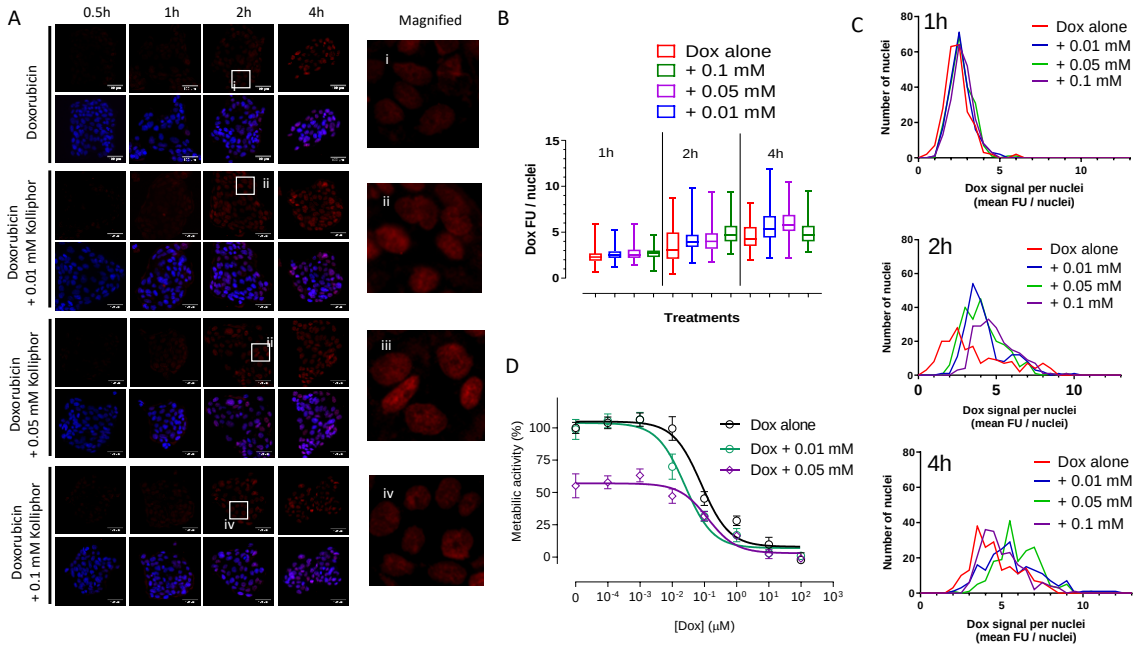

Figure 6. Doxorubicin intracellular exposure and potency on co-application of surfactant in Calu-3 cells. (A) Fluorescent micrographs of doxorubicin (red) and DAPI nuclear stain (blue) shown in rows. Images labelled i, ii, iii and iv are enlarged areas highlighted by boxes. Scale bars, 100 µm. (B) Data analysis showing levels of doxorubicin (Dox) fluorescence calculated *per* nucleus and represented as mean ± S.D (as described in Supporting information Figure S6). (C) Distribution profiles of doxorubicin fluorescence per nucleus at

different time points. Associated histograms shown in Supporting information Figure S7. (D) Effect of surfactant co-administration on doxorubicin potency determined by PrestoBlue metabolic activity assay. Data presented as mean ± S.D and dose-response curve fitted using GraphPad Prism.

We also considered if increased nuclear level of doxorubicin may not be arising solely from increased permeability of plasma and nuclear membranes, as shown above, but also due to potential effect of surfactant on P-glycoprotein (P-gp) membrane transporter [30, 31], a known efflux pump of doxorubicin [44]. The experiment is summarized in Supporting Information (Figure S8) and demonstrates that exposure of Calu-3 cells to the surfactant results in a concentration-dependent reduction in P-gp activity. Interestingly, the reductions in P-gp activity occurs below the surfactant's CMC, indicating its relationship with surfactant inclusion into membrane lipid bilayer, and its contribution to internalization of doxorubicin. It should be noted here that Calu-3 expression of P-gp has been reported to be low relative to other epithelial cell lines, including airway A549 and intestinal Caco-2 [45] . It could therefore be proposed that Calu-3 model may be underestimating the potential of surfactant-mediated enhancement of doxorubicin cellular bioavailability due to inhibition of P-gp.

Considering doxorubicin potency (Figure 6d), IC_{50} of doxorubicin applied alone in Calu-3 cells was determined to be 80.1 ± 13.1 nM. Treatments with doxorubicin in the presence of surfactant result in following effects; co-administration at 0.01 mM concentration (below surfactant CMC) results in a significant ($P<0.01$), 3-fold increase in doxorubicin potency with an IC_{50} of 24.9 ± 8.4 nM, and can be corroborated with an increased membrane permeability seen at concentrations below the CMC (Figure 2), whilst significant toxicity was observed at higher surfactant concentrations (Supporting Information Figure S9), which consequently makes deciphering the data ambiguous, as illustrated in Figure 6d by the profile for 0.05 mM doxorubicin and surfactant co-tretment.

4. Discussion

Our initial experiment visualises modulation in cell plasma membrane lipid bilayer ordered (L_o) and disordered (L_D) regions on exposure to amphiphilic surfactant (Figure 1). The magnitude of the observed increase in liquid disorder of cell plasma membrane is shown to increase as the concentration of surfactant increases. Further evidence of surfactant action on the cell plasma membrane, and on model membrane of giant liposomes, arrives from assessment of the membrane fluidity, *via* employment of the classical Laurdan probe. In this experiment, we show that exposure to surfactant results in statistically significant, concentration-dependent increase in membrane fluidity. The GP value reflects lipid bilayer packing, and a decrease in GP on surfactant exposure clearly points to an increase in membrane fluidity i.e. increased water presence and lower packing order [46] of cell plasma and liposomal lipid bilayers upon surfactant exposure. It should be noted that surfactant induced increases in membrane bilayer disorder occur even below the critical micellar concentration (CMC) of the employed surfactant (Kolliphor® HS15), which lies between

0.05 – 0.1 mM, as we determined previously [10], and is similar to values reported in the literature (0.05- 0.2 mM) [47] (Figure 2).

In the next step we assessed if increased bilayer disorder is, at least in part, arising from insertion of surfactant molecules into the membrane lipid bilayer. We again used giant liposomes with a lipid bilayer composition modelling that of epithelial cell plasma membrane (Figure 3). The experiment demonstrates time-dependent effects of surfactant on the liposome morphology, whereby the first observable morphological change is budding of the liposomal membrane (membrane expanding outwards). Budding of this nature is normally considered to be the membrane's outer leaflet protrusion on insertion of surfactant molecules to outer leaflet of the lipid bilayer. The phenomenon is attributed to surfactant molecules partition into the bilayer's outer leaflet which, due to their trans-bilayer diffusion (flip-flop) being relatively slow, results in asymmetric expansion of the bilayer [48]. For amphiphilic surfactants, as used in this study, the head group attributes appear to strongly influence trans-bilayer diffusion rates, with half-times ranging from 350 ms to several hours, as estimated for octaethylene glycol monododecyl ether or dodecylmaltoside, respectively [28, 49]. In agreement with the previous report on giant liposomes comprising of phosphocholine/sphingomyelin/cholesterol, and treated with non-ionic surfactants (Triton X-100 and Brij 98), bilayer budding in our study also eventually leads to the formation of smaller vesicles [48]. It should be noted however that even at the surfactant concentration significantly above the CMC (5.2 mM *vs* 0.05 – 0.1 mM, respectively), a full solubilisation of the giant liposomes into mixed micelles, consisting of dissolved lipids and surfactant, was not observed, as one would expect from the generally accepted surfactant-membrane interaction model [50, 51]. As a comparison to the work by Mui et al. [48], we exposed our giant liposome model to Triton X-100 and also observed incomplete liposomal solubilisation and remnant smaller vesicles (Supporting Information Figure S10). As fluorescent microscopy used to assess morphology of giant liposomes (Figure 3) does not have a resolution required to visualise potential presence of the proposed mixed micelles, possibly forming due to surfactant effect on the lipid bilayer membrane, a supplementary experiment using liposomes of the same membrane composition to the giant liposomes, but fabricated in sub-micron size – appropriate for dynamic light scattering analysis was conducted. It indeed reveals formation of a population of species in 13 - 14 nm size range (radius), not present in liposomes or surfactant only samples, and indicative of a process of liposomes 'solubilisation' [50,51] (Supporting Information Figure S11).

In a further experiment, we observed morphological changes indicative of surfactant insertion into outer leaflet of a cell membrane in experiment using erythrocytes, whereby echinocytic form of 'affected' and a sub-population of not 'affected' (discocyte) erythrocytes are observed. Similar membrane budding on surfactant exposure was also observed in epithelial cells (Figure 3).

It is important to note that the observed budding indicates that insertion of the surfactant molecules into the lipid bilayer membrane is spatially non-homogeneous (Figure 3). A non-homogeneity is also observed in images of Laurdan fluorescence emission in giant liposomes,

as well as in the Calu-3 cell culture model, as depicted in Figure 2. Similar localized modulation of the lipid bilayer structure has been described previously and termed 'heterogeneous perturbation' [52], and the proposed explanation suggests that poor mixing of the surfactant with the lipid layer leads to segregation and formation of surfactant rich clusters that disrupt membrane locally.

Comparing the experiments above, the phenomenon of membrane 'patches' with high levels of fluidity is manifested in both giant liposome and cell culture models (Figure 2). This suggested that spatially heterogeneous surfactant insertion, as seen in giant liposomes, may be also occurring in cells exposed to the surfactant, as is observed in erythrocytes as well as in epithelial cells (Figure 3). Laurdan fluidity measurements in cells exposed to the surfactant suggest that this would already occur at concentrations bellow the CMC of the surfactant.

We further show that surfactant exposure results in cholesterol extraction from cell plasma membrane (Figure 4), the process that would contribute to an increase in membrane fluidity, but that here a statistically significant extraction is measured at surfactant concentrations that are above its CMC. This suggests that cholesterol depletion from lipid bilayer membrane occurs through its incorporation into surfactant micelles - appearing as an additional peak with mean radius of around 13 – 14 nm, in addition to surfactant micelles peak at approximately 7 nm (Figure S11, Supporting information). Similarly, a reduction in cholesterol content of erythrocyte membrane was reported to occur on application of Triton X-100 at concentrations greater than its CMC [53], although Kolliphor HS15 and Triton X-100 would have different critical packing parameters, and therefore the effects on membrane perturbation could be expected to differ somewhat. Taken together, the data hence indicate that an increase in membrane fluidity occurs already at concentrations below the surfactant's CMC, attributable to its insertion into the membrane, while at concentrations above the CMC the cholesterol depletion from the membrane further contributes to the trend.

Our results presented so far demonstrate insertion of the surfactant into the membrane lipid bilayer (Figure 3), increased membrane bilayer fluidity (Figure 2), extraction of cholesterol from the lipid bilayer (Figure 4), and the changes in plasma membrane lipid domains (Figure 1), all contributing to the observed increased membrane permeability (Figure 5), and all demonstrating surfactant concentration-dependency. Similarly, concertation dependent increase in membrane permeability on surfactant exposure has been reported in many studies since early reports in the 1980s [11, 54]. Our study further illustrates that, in line with increased permeability, there is an increased doxorubicin 'dosing' in nuclei of cells exposed to surfactant at concentrations even below the CMC (0.01 and 0.05 mM) as well as close (0.1 mM) to the surfactant's CMC (0.05 – 0.1 mM) (Figure 6). Furthermore, increased overall doxorubicin potency is observed, with a statistically significant, 3-fold reduction in doxorubicin IC_{50} in cells co-treated with 0.01 mM surfactant (Figure 6d). Importantly, this indicates that increased cell plasma and nuclear membrane permeabilities to a permeant of doxorubicin properties, and its consequent increased intracellular 'dosing', can be achieved in the presence of surfactant at relatively low concentrations, below surfactant CMC. This fact has implications to adoption and design of permeability enhancers as pharmaceutical

formulations technology, as well as nature of corresponding cell toxicity caused by the surfactant [9,55].

What is of considerable importance is to note that images in Figure 5b and c and plots in Figure 6c, clearly illustrate heterogeneity of the measured effects in the cell population. Although distribution profiles in Figure 6c show a shift towards higher doxorubicin 'dosing *per* nucleus' for cells co-treated with surfactant, the broad curve profile indicates that even on surfactant co-treatment a heterogenous dosing level to the cells in population exists.

Currently it is unclear what may be causing the observed heterogeneity in surfactant effects at cell population level. Contributing factors may be different stages in cell proliferation, which is shown to affect cell membrane lipid composition and dynamics [56]. However, the variability may also be a consequence of cellular crowding and cell-cell interactions (as seen in Figures 1 and 5), factors reported to influence plasma membrane composition and cell behaviour in cell population [57, 58]. These may result in discreet cell sub-populations having different levels of susceptibility to surfactant interaction and effect.

One should recognise here the importance of plasma membrane polarization in epithelial cells in tissue layers [59], as well as differences in plasma membrane composition in epithelial cells at different locations in the body [60, 61], both necessitating further studies, from the observations presented here, on epithelial tissue relevant to a specific therapeutic site.

Taken together, throughout the study the experiments conducted point to heterogeneity in surfactant effects at the cell membrane, as well as at cell population level.

Conclusion

In this study we conducted experiments in parallel, as technically feasible, in cells and in giant liposomes modelling cell plasma membrane composition, to allows us to gain further mechanistic understanding of amphiphilic surfactant behaviour and effects. Our results show that changes in membrane fluidity initially occur upon insertion of individual surfactant molecules (i.e. at concentrations below surfactant CMC) into the lipid bilayer. Contrastingly, the sequestration of cholesterol, an effect also contributing to changes in membrane structure, requires surfactant concentrations above the CMC. The study further shows that surfactant insertion, and related increase in membrane fluidity, are heterogeneous; i.e. 'patches' of increased membrane fluidity are observed. At the cell population level, the data also show heterogeneous effects of surfactant exposure, with cells of high permeability amongst the 'background' population. We propose that this heterogeneity is further manifested in a broad 'intracellular dosing' profile of model drug in the cell population. The study provides new mechanistic insight into the interaction of surfactants with cells at cell membrane and cells in population levels.

Acknowledgements

The authors acknowledge funding obtained from BBSRC Grant BB/H016538/1 and MRC Grant 1872576.

References

1. Aungst, B. J.; Saitoh, H.; Burcham, D. L.; Huang, S.-M.; Mousa, S. A.; Hussain, M. A., Enhancement of the intestinal absorption of peptides and nonpeptides. *Journal of Controlled Release* **1996,** *41* (1–2), 19-31.
2. Gamboa, J. M.; Leong, K. W., In vitro and in vivo models for the study of oral delivery of nanoparticles. *Advanced Drug Delivery Reviews* **2013,** *65* (6), 800-810.
3. Makhlof, A.; Tozuka, Y.; Takeuchi, H., Design and evaluation of novel pH-sensitive chitosan nanoparticles for oral insulin delivery. *European Journal of Pharmaceutical Sciences* **2011,** *42* (5), 445-451.
4. Brayden, D. J.; Hill, T. A.; Fairlie, D. P.; Maher, S.; Mrsny, R. J., Systemic delivery of peptides by the oral route: Formulation and medicinal chemistry approaches. *Adv Drug Deliv Rev* **2020,** *157*, 2-36.
5. Vllasaliu, D.; Shubber, S.; Fowler, R.; Garnett, M.; Alexander, C.; Stolnik, S., Epithelial toxicity of alkylglycoside surfactants. *Journal of Pharmaceutical Sciences* **2013,** *102* (1), 114-125.
6. Lin, H.; Gebhardt, M.; Bian, S.; Kwon, K. A.; Shim, C.-K.; Chung, S.-J.; Kim, D.-D., Enhancing effect of surfactants on fexofenadine·HCl transport across the human nasal epithelial cell monolayer. *International Journal of Pharmaceutics* **2007,** *330* (1–2), 23-31.
7. McCartney, F.; Rosa, M.; Brayden, D. J., Evaluation of Sucrose Laurate as an Intestinal Permeation Enhancer for Macromolecules: Ex Vivo and In Vivo Studies. *Pharmaceutics* **2019,** *11* (11).
8. Gleeson, J. P.; Frias, J. M.; Ryan, S. M.; Brayden, D. J., Sodium caprate enables the blood pressure-lowering effect of Ile-Pro-Pro and Leu-Lys-Pro in spontaneously hypertensive rats by indirectly overcoming PepT1 inhibition. *Eur J Pharm Biopharm* **2018,** *128*, 179-187.
9. Cavanagh, R. J.; Smith, P. A.; Stolnik, S., Exposure to a Nonionic Surfactant Induces a Response Akin to Heat-Shock Apoptosis in Intestinal Epithelial Cells: Implications for Excipients Safety. *Mol Pharm* **2019,** *16* (2), 618-631.
10. Shubber, S.; Vllasaliu, D.; Rauch, C.; Jordan, F.; Illum, L.; Stolnik, S., Mechanism of mucosal permeability enhancement of CriticalSorb(R) (Solutol(R) HS15) investigated in vitro in cell cultures. *Pharm Res* **2015,** *32* (2), 516-27.
11. Twarog, C.; Fattah, S.; Heade, J.; Maher, S.; Fattal, E.; Brayden, D. J., Intestinal Permeation Enhancers for Oral Delivery of Macromolecules: A Comparison between Salcaprozate Sodium (SNAC) and Sodium Caprate (C10). *Pharmaceutics* **2019,** *11* (2).
12. Pomorski, T. G.; Nylander, T.; Cárdenas, M., Model cell membranes: Discerning lipid and protein contributions in shaping the cell. *Advances in Colloid and Interface Science* **2014,** *205* (0), 207-220.
13. Singer, S. J.; Nicolson, G. L., The Fluid Mosaic Model of the Structure of Cell Membranes. *Science* **1972,** *175* (4023), 720-731.
14. Anderson, R. G. W.; Jacobson, K., A Role for Lipid Shells in Targeting Proteins to Caveolae, Rafts, and Other Lipid Domains. *Science* **2002,** *296* (5574), 1821-1825.
15. Douglass, A. D.; Vale, R. D., Single-Molecule Microscopy Reveals Plasma Membrane Microdomains Created by Protein-Protein Networks that Exclude or Trap Signaling Molecules in T Cells. *Cell* **2005,** *121* (6), 937-950.
16. Elson, E. L.; Fried, E.; Dolbow, J. E.; Genin, G. M., Phase Separation in Biological Membranes: Integration of Theory and Experiment. *Annual Review of Biophysics* **2010,** *39* (1), 207-226.

17. Rajendran, L.; Simons, K., Lipid rafts and membrane dynamics. *Journal of Cell Science* **2005,** *118* (6), 1099-1102.
18. van Meer, G., Voelker, Dennis R, Feigenson, Gerald W., Membrane lipids: where they are and how they behave. *Nat Rev Mol Cell Biol* **2008,** *9* (2), 12.
19. Arouri, A.; Mouritsen, O. G., Membrane-perturbing effect of fatty acids and lysolipids. *Progress in Lipid Research* **2013,** *52* (1), 130-140.
20. Busch, S.; Unruh, T., The influence of additives on the nanoscopic dynamics of the phospholipid dimyristoylphosphatidylcholine. *Biochimica Et Biophysica Acta-Biomembranes* **2011,** *1808* (1), 199-208.
21. Shibata, H.; Saito, H.; Yomota, C.; Kawanishi, T.; Okuda, H., Alterations in the Detergent-Induced Membrane Permeability and Solubilization of Saturated Phosphatidylcholine/Cholesterol Liposomes: Effects of Poly(ethylene glycol)-Conjugated Lipid. *Chemical & Pharmaceutical Bulletin* **2012,** *60* (9), 1105-1111.
22. Suwalsky, M.; Mennickent, S.; Norris, B.; Villena, F.; Sotomayor, C. P., Effects of the antiepileptic drug carbamazepine on human erythrocytes. *Toxicology in Vitro* **2006,** *20* (8), 1363-1369.
23. Liu, X.-Y.; Yang, Q.; Kamo, N.; Miyake, J., Effect of liposome type and membrane fluidity on drug–membrane partitioning analyzed by immobilized liposome chromatography. *Journal of Chromatography A* **2001,** *913* (1), 123-131.
24. Zhang, L.; Rozek, A.; Hancock, R. E., Interaction of cationic antimicrobial peptides with model membranes. *Journal of Biological Chemistry* **2001,** *276* (38), 35714-35722.
25. Schreier, S.; Malheiros, S. V.; de Paula, E., Surface active drugs: self-association and interaction with membranes and surfactants. Physicochemical and biological aspects. *Biochimica et Biophysica Acta (BBA)-Biomembranes* **2000,** *1508* (1), 210-234.
26. Helenius, A.; Simons, K., Solubilization of membranes by detergents. *Biochimica et biophysica acta* **1975,** *415* (1), 29-79.
27. le Maire, M.; Champeil, P.; Møller, J. V., Interaction of membrane proteins and lipids with solubilizing detergents. *Biochimica et Biophysica Acta (BBA) - Biomembranes* **2000,** *1508* (1–2), 86-111.
28. Kragh-Hansen, U.; le Maire, M.; Møller, J. V., The mechanism of detergent solubilization of liposomes and protein-containing membranes. *Biophysical journal* **1998,** *75* (6), 2932-2946.
29. Lichtenberg, D.; Robson, R. J.; Dennis, E. A., Solubilization of phospholipids by detergents. Structural and kinetic aspects. *Biochimica et biophysica acta* **1983,** *737* (2), 285-304.
30. Strickley, R. G., Solubilizing excipients in oral and injectable formulations. *Pharm Res* **2004,** *21* (2), 201-30.
31. Brayden, D. J.; Bzik, V. A.; Lewis, A. L.; Illum, L., CriticalSorb promotes permeation of flux markers across isolated rat intestinal mucosae and Caco-2 monolayers. *Pharm Res* **2012,** *29* (9), 2543-54.
32. Spink, C. H.; Yeager, M. D.; Feigenson, G. W., Partitioning behavior of indocarbocyanine probes between coexisting gel and fluid phases in model membranes. *Biochim Biophys Acta* **1990,** *1023* (1), 25-33.
33. Huang, N. N.; Florine-Casteel, K.; Feigenson, G. W.; Spink, C., Effect of fluorophore linkage position of n-(9-anthroyloxy) fatty acids on probe distribution between coexisting gel and fluid phospholipid phases. *Biochim Biophys Acta* **1988,** *939* (1), 124-30.
34. Owen, D. M.; Rentero, C.; Magenau, A.; Abu-Siniyeh, A.; Gaus, K., Quantitative imaging of membrane lipid order in cells and organisms. *Nat. Protocols* **2012,** *7* (1), 24-35.
35. Szoka, F., Jr.; Papahadjopoulos, D., Comparative properties and methods of preparation of lipid vesicles (liposomes). *Annual review of biophysics and bioengineering* **1980,** *9*, 467-508.
36. Velegaleti, R., Ku, S., Solutol HS15 as a Novel Excipient. *Pharmaceutical Technology* **2010,** *34* (11).

37. Sanchez, S. A.; Tricerri, M. A.; Gratton, E., Laurdan generalized polarization fluctuations measures membrane packing micro-heterogeneity in vivo. *Proc Natl Acad Sci U S A* **2012,** *109* (19), 7314-9.
38. Harris, F. M.; Best, K. B.; Bell, J. D., Use of laurdan fluorescence intensity and polarization to distinguish between changes in membrane fluidity and phospholipid order. *Biochim Biophys Acta* **2002,** *1565* (1), 123-8.
39. Heerklotz, H., Interactions of surfactants with lipid membranes. *Q Rev Biophys* **2008,** *41* (3-4), 205-64.
40. Keller, S.; Tsamaloukas, A.; Heerklotz, H., A quantitative model describing the selective solubilization of membrane domains. *J Am Chem Soc* **2005,** *127* (32), 11469-76.
41. Iglic, A.; Kralj-Iglic, V., Hägerstrand, H., Stability of spiculated red blood cells induced by intercalation of amphiphiles in cell membrane. Med Biol Eng Comput. 1998; 36(2):251..
42. Simons, K.; Ikonen, E., Functional rafts in cell membranes. *Nature* **1997,** *387* (6633), 569-572.
43. Maxfield, F. R.; Wustner, D., Analysis of cholesterol trafficking with fluorescent probes. *Methods Cell Biol* **2012,** *108*, 367-93.
44. Krishna, R.; Mayer, L. D., Multidrug resistance (MDR) in cancer. Mechanisms, reversal using modulators of MDR and the role of MDR modulators in influencing the pharmacokinetics of anticancer drugs. *Eur J Pharm Sci* **2000,** *11* (4), 265-83.
45. Hamilton, K. O.; Backstrom, G.; Yazdanian, M. A.; Audus, K. L., P-glycoprotein efflux pump expression and activity in Calu-3 cells. *J Pharm Sci* **2001,** *90* (5), 647-58.
46. Carradori, D.; Dos Santos, A. G.; Masquelier, J.; Paquot, A.; Saulnier, P.; Eyer, J.; Preat, V.; Muccioli, G. G.; Mingeot-Leclercq, M. P.; des Rieux, A., The origin of neural stem cells impacts their interactions with targeted-lipid nanocapsules: Potential role of plasma membrane lipid composition and fluidity. *J Control Release* **2018,** *292*, 248-255.
47. BASF *Kolliphor® HS 15: Technical Information.*; 2020.
48. Mui, B. L.; Döbereiner, H. G.; Madden, T. D.; Cullis, P. R., Influence of transbilayer area asymmetry on the morphology of large unilamellar vesicles. *Biophysical Journal* **1995,** *69* (3), 930-941.
49. Le Maire, M.; Moeller, J. V.; Champeil, P., Binding of a nonionic detergent to membranes: flip-flop rate and location on the bilayer. *Biochemistry* **1987,** *26* (15), 4803-4810.
50. Lichtenberg, D.; Robson, R. J.; Dennis, E. A., Solubilization of phospholipids by detergents structural and kinetic aspects. *Biochimica et Biophysica Acta (BBA) - Reviews on Biomembranes* **1983,** *737* (2), 285-304.
51. Kragh-Hansen, U.; Le Maire, M.; Møller, J. V., The mechanism of detergent solubilization of liposomes and protein- containing membranes. *Biophysical Journal* **1998,** *75* (6), 2932-2946.
52. Nazari, M.; Kurdi, M.; Heerklotz, H., Classifying surfactants with respect to their effect on lipid membrane order. *Biophys J* **2012,** *102* (3), 498-506.
53. Kirkpatrick, F. H.; Gordesky, S. E.; Marinetti, G. V., Differential solubilization of proteins, phospholipids, and cholesterol of erythrocyte membranes by detergents. *Biochim Biophys Acta* **1974,** *345* (2), 154-61.
54. Ueno, M., Partition behavior of a nonionic detergent, octyl glucoside, between membrane and water phases, and its effect on membrane permeability. *Biochemistry* **1989,** *28* (13), 5631-4.
55. McCartney, F.; Gleeson, J. P.; Brayden, D. J., Safety concerns over the use of intestinal permeation enhancers: A mini-review. *Tissue Barriers* **2016,** *4* (2), e1176822.
56. Denz, M.; Chiantia, S.; Herrmann, A.; Mueller, P.; Korte, T.; Schwarzer, R., Cell cycle dependent changes in the plasma membrane organization of mammalian cells. *Biochim Biophys Acta Biomembr* **2017,** *1859* (3), 350-359.
57. Snijder, B.; Pelkmans, L., Origins of regulated cell-to-cell variability. *Nat Rev Mol Cell Biol* **2011,** *12* (2), 119-25.

58. Frechin, M.; Stoeger, T.; Daetwyler, S.; Gehin, C.; Battich, N.; Damm, E. M.; Stergiou, L.; Riezman, H.; Pelkmans, L., Cell-intrinsic adaptation of lipid composition to local crowding drives social behaviour. *Nature* **2015,** *523* (7558), 88-91.
59. van, I. S. C. D.; Agnetti, J.; Gassama-Diagne, A., Mechanisms behind the polarized distribution of lipids in epithelial cells. *Biochim Biophys Acta Biomembr* **2020,** *1862* (2), 183145.
60. Brasitus, T. A.; Dudeja, P. K., Regional differences in the lipid composition and fluidity of rat colonic brush-border membranes. *Biochim Biophys Acta* **1985,** *819* (1), 10-7.
61. Ibrahim, S. A.; Balasubramanian, K. A., Lipid composition and membrane fluidity of monkey small intestinal brush border membrane: regional differences. *Indian J Biochem Biophys* **1995,** *32* (5), 290-4.